Improving sound transmission loss at ring frequency of a curved panel using tunable 3D-printed small-scale resonators

Christophe Droz, Olivier Robin, Mohamed Ichchou, Noureddine Atalla

Improving sound transmission loss at ring frequency of a curved panel using tunable 3D-printed small-scale resonators

Christophe Droz,[1, a)] Olivier Robin,[2] Mohamed Ichchou,[1] and Noureddine Atalla[2]

[1)] *Vibroacoustics & Complex Media Research Group, LTDS - CNRS UMR 5513, École Centrale de Lyon, France*

[2)] *Groupe d'acoustique de l'université de Sherbrooke, Université de Sherbrooke, 2500, boulevard de l'université, Sherbrooke, Canada J1K 2R1*

christophe.droz@ec-lyon.fr,

olivier.robin@usherbrooke.ca,

mohamed.ichchou@ec-lyon.fr,

noureddine.atalla@usherbrooke.ca

(Dated: 21 November 2018)

Abstract: An important dip in the sound transmission loss of curved panels occurs at the ring frequency. The relevance of using small-scale resonators to solve this issue is experimentally demonstrated on an aircraft sidewall panel. The effect of varying the spatial distribution of single frequency resonators (including combination with a broadband soundproofing treatment), as well as using multi-frequency resonators with a fixed spatial distribution is studied. Large improvement of the measured sound transmission loss under a diffuse acoustic field excitation is obtained around the ring frequency with limited added mass and very small alteration of the overall sound insulation performance.

Keywords: Vibration control; Curved panel; Sound Transmission Loss; Small-scale resonator; Ring frequency; Diffuse Acoustic Field

[a)]Author to whom correspondence should be addressed.

1. Introduction

The design of lightweight and efficient soundproofing packages is one of the top priorities in the general transportation industry for noise, vibration and harshness objectives. A very common solution to this weight-efficiency compromise is the use of light porous material attachments on structures, the latter being usually simplified or modelled as flat whereas they can have a variable curvature radius in reality (a ship hull, an aircraft cabin). In usual sound transmission loss (STL) results for cylindrical shells under a diffuse acoustic field (DAF) excitation[1], a first noticeable STL reduction occurs at the cylinder ring frequency which is a function of the shell radius and longitudinal waves velocity. A second dip in STL results happens at the coincidence frequency where structural and acoustic wavenumbers coincide (common to both curved and plane structures). Classical porous treatments that mainly provides broadband sound attenuation are not optimal for solving these reductions of sound insulation performance in narrow frequency bandwidths. Moreover, for typical aircraft sidewalls, the ring frequency-related dip occurs at low frequency (typically 400 to 800 Hz).

The design of ribbed or stiffened structures can be optimized to modify the frequency bandwidth affected by the two previously cited specific frequencies[2]. A large variety of passive or active solutions have also been proposed. A typical example of an active approach for controlling acoustic transmissibility of aircraft panels is decentralized active control with distributed units[3,4]. Concerning passive solutions and apart from the classical solution of increasing the panel's structural damping, innovative approaches to tonal or narrow-band

problems have been largely inspired by recent research on locally resonant metamaterials and often involve the use of periodic add-on units. The locally resonant bandgaps obtained using either Helmholtz resonators[5,6], periodically distributed tuned mass dampers[7] or surface-mounted resonators[8,9] can be used to improve the STL. For composites plates in which the coincidence frequency zone is usually larger than for a single layer homogeneous plate, a possible solution is then to use multi-modal resonators to broaden stop-bands[10]. Excepting Ref.[5], a commonality in previously cited references[6–10] is that only plane structures and then coincidence frequency are considered. To the best of the authors' knowledge, the reduction of the negative impact of the ring mode on the STL of a curved panel by means of a passive, tunable and multi-resonant approach has not yet been published. In this work, a tunable resonator concept involving 3D-printed cantilever beams with variable tip end magnets is experimentally studied on an aircraft sidewall panel including stringer and ring frame attachments under a DAF excitation. Several spatial distributions of the resonators including a multi-resonant configuration as well as possible addition of this narrow-band solution to a broadband sound absorbing treatment are investigated.

2. Proposed design of tunable 3D-printed cantilever small-scale resonators

The proposed small-scale resonators are based on a 3D-printed core structure using polycarbonate polymer consisting in a beam of section $10\times4\,\mathrm{mm}^2$ and length 23 mm supported by a stiffener of section $4\times3.5\,\mathrm{mm}^2$ (see various illustrations in Figs. 1(a-e)). The base part is a cube of $10\times10\times8\,\mathrm{mm}^3$ dimensions on which the beam and the stiffener are both connected. The connection to the structure is made at the base using a sealant (see Fig. 1(d)). The

overall unit volume occupied by a resonator without a tuning mass is finally $33\times10\times8\,\mathrm{mm}^3$, with a unit weight of 2.72 g.

A 1 mm-thick base magnet is glued at the tip end and the resonators are then tuned using different neodymium magnets of known masses. The tuning masses and corresponding resonance frequencies for the resonators shown in Figs. 1(a-c) are 2.24 g and 670 Hz (F1), 1.11 g and 820 Hz (F2), and 0.74 g and 980 Hz (F3), respectively. These average resonance frequencies were estimated on a few numbers of resonators when installed on the tested panel using a laser Doppler vibrometer and a shaker excitation.

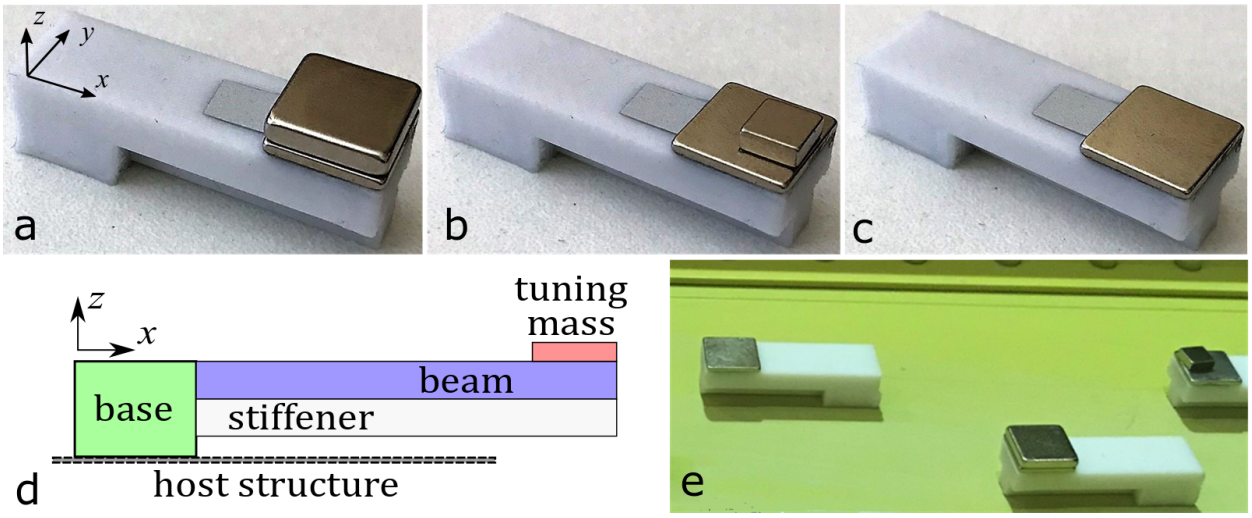

Fig. 1. (Color online) Pictures and schematic of the small-scale resonators. (a) Resonator F1. (b) Resonator F2. (c) Resonator F3. (d) Schematic describing the resonator parts. (e) Close-up view of the three resonators types mounted on a panel.

3. Experimental methods and tested configurations

According to standards[11,12], STL is determined in coupled reverberant-anechoic rooms using measurements of the spatially averaged sound pressure level in the source room L_p and of the spatially averaged average sound intensity level L_i over a scanning surface S_m on the receiving side (both in dB), STL $= L_p - L_i - 6 - 10\log_{10}(S_m/S)$ (with S the effective panel area, considered equal to the scanning area S_m considered equal so that the last term was neglected). All measurements were conducted in the coupled reverberant-anechoic rooms at groupe d'acoustique de l'Université de Sherbrooke. A DAF excitation was generated in the reverberant room ($7.2 \times 6.5 \times 3$ m^3 dimensions) using a loudspeaker with a white noise input in the $50 - 5000$ Hz frequency range. The average sound pressure level in the reverberant room L_p was obtained by rotating a half-inch PCB microphone with more than a complete rotation of its supporting arm during the signal acquisition time (of 120 seconds for each test). The average radiated sound intensity level L_i was measured in the anechoic room ($6.8 \times 6.5 \times 3$ m^3 dimensions) using a Bruel & Kjaer sound intensity probe composed of two half-inch microphones and a 12 mm spacer. Manual scanning was performed at a distance of 10 cm from the panel surface following recommended scan patterns[11,12]. Standards[11,12] also recommend not exceeding a pressure-intensity indicator value of 10 dB for a sound-reflecting test specimen which was verified in each measurement. Finally, all the results presented hereinafter are provided in 12^{th} octave bands between 150 and 5000 Hz.

The structure under test is a curved rectangular fuselage panel equipped with axial and circumferential stiffeners (see Figure 2(a)). The panel is made of 1.27 mm-thick aeronautic grade aluminum with a 21.4 kg total weight. Its length is 1.7 m with outer and inner

circumferences of 1.45 m and 1.3 m, respectively. Its curvature radius is approximately 1.6 m. The equivalent mass per unit area of the fuselage equipped with attachments is approximately 8.68 $\mathrm{kg.m^{-2}}$ while the bare aluminum shell has a theoretical 3.43 $\mathrm{kg.m^{-2}}$ mass per unit area. The panel was mounted in the test window using a frame made of plywood with acoustic sealing made of neoprene adhesive and silicone. The frame and surrounding surfaces were covered with a sound insulating barrier including an open-cell sound absorbing material and a PVC heavy layer.

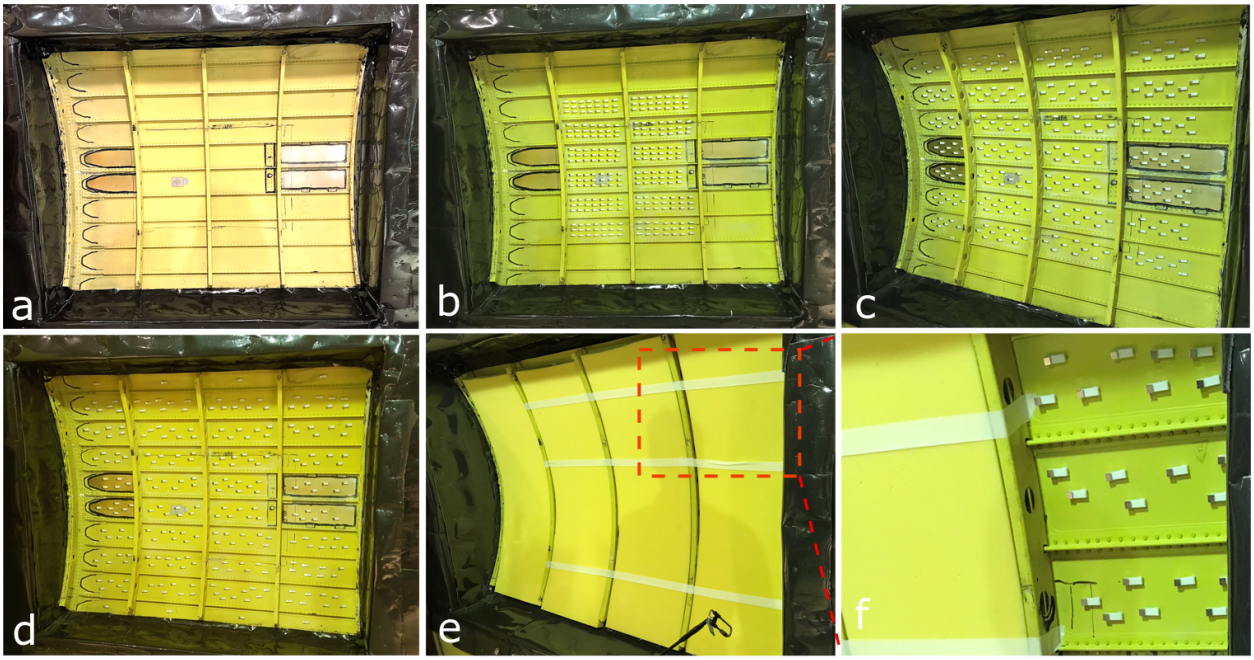

Fig. 2. (Color online) Pictures of the tested configurations. (a) Bare panel. (b) D1 distribution of resonators. (c) D2 distribution of resonators. (d) D3 distribution of resonators. (e) Panel fully covered by melamine foam. (f) Close-up view of the panel equipped with D3 distribution of resonators prior mounting of the lateral melamine foam piece.

The tested configurations are visually displayed and summarized in Figs. 2(a-f). Fig. 2(a) corresponds to the reference configuration, *i.e.* the bare panel, with measurements conducted both at the beginning and at the end of the series of experiments in order to verify repeatability and data consistency. The difference between those two tests was below 0.5 dB per 12^{th} octave band. For all tests, the resonators were bonded on the panel skin with wax typically used to mount accelerometers. Fig. 2(b) illustrates the D1 distribution of resonators. In this case, 246 resonators are placed on the central portion of the panel (21 or 18 resonators per bay on 12 bays). The D2 distribution of resonators is depicted in Fig. 2(c). The available 246 resonators are now distributed on the panel at the exception of upper and lower parts of the panel, with 7 to 10 resonators per bay on 28 bays. Fig. 2(d) illustrates the D3 distribution of resonators that now fully cover the panel area. The number of resonators per bay varies between 5 and 9 for a total number of 240 resonators on 32 bays (including one additional resonator on each of the 8 upper and lower edges' bays). The choice of these configurations is mainly empirical for this first proof-of-concept.

The positioning of a sound absorbing treatment over the panel area is finally shown in Figure 2(e) (including possible combination with the D3 distribution of resonators). A melamine foam of 50.8 mm thickness was chosen to study its effect on measured STL when used alone or combined with resonators. This material has a mass density of 6.1 kg/m^3, a static air flow resistivity of 7920 Ns/m^4, a tortuosity of 1, a porosity of 0.98 and viscous and thermal lengths of 132 μm and 149 μm, respectively. Four foam layers of dimensions 1.34 m $\times$ 0.37 m are inserted between the circumferential stiffeners, supported by stringers

and kept in place with tape (see Figure 2(e)). Since the resonators have a smaller height than the stringers, the resonators are not in contact with the foam layer. The total added mass for the foam is 0.6 kg. Figure 2(f) presents a close-up view of the panel equipped with resonators prior complete installation of the melamine foam.

All the tested configurations are summarized in Table 1 with corresponding percent added mass and figure result number. Using only F1 resonators, the D1, D2 and D3 distributions are first tested (see Figs. 2(b,c,d), respectively). Based on the D2 distribution (Fig. 2(c)), combinations of F1, F2 and F3 resonators are then used to produce a multi-modal locally resonant add-on covering the anti-resonance region. Note that although the number of resonators remains unchanged for the three configurations, the added mass is slightly decreased in the multi-modal configuration, as F2 and F3 resonators are lighter than F1 resonators (see Table 1). The effect of the sound absorbing treatment is finally tested alone and in combination with the D3 distribution of resonators in single mode (F1).

4. Experimental results and discussions

Results obtained are reported in Figs. 3(a-d). The reference STL curve for the bare panel is systematically included in Figs. 3(a-c) in order to ease comparison between test cases described in Table 1. In Figure 3(d), the effect of four key configurations is also plotted in terms of insertion loss so as to highlight STL improvement brought by each setup.

A theoretical ring frequency f_r of approximately 530 Hz is calculated using the simplified relation for a non stiffened thin shell[1] $f_r = \sqrt{E/\rho(1-\nu^2)}/(2\pi r)$, with E the Young's modulus (= 70 GPa), ρ the mass density (= 2700 kg/m^3), ν the Poisson's ratio (= 0.3) and

Table 1. Summary of tested configurations.

Tested configuration [**results figure number**]	Number of resonators F1	F2	F3	**Total** and tip end mass (both in kg)	Foam	Total added mass (%)
D1, D2 and D3 distributions, single mode (F1) [**Fig.3(a-b-c)**]	246	0	0	**1.22**, 0.55	No	5.7
D2 distribution, Two modes (F1-F2) [**Fig.3(b)**]	142	104	0	**1.10**, 0.43	No	5.15
D2 distribution, Three modes (F1-F2-F3) [**Fig.3(b)**]	116	87	43	**1.05**, 0.39	No	4.9
D3 distribution, Single mode (F1) [**Fig.3(c)**]	246	0	0	**1.82**, 0.55	Yes	8.5
Foam alone [**Fig.3(c)**]	0	0	0	**0.6**, -	Yes	2.8

r the curvature radius. This approximated f_r is indicated by a vertical arrow in Figure 3(a), and the largest decrease of measured STL is obtained above this frequency at the 630 and 670 Hz twelfth octave bands. This bias might be explained by the fact that the mass density of the panel skin alone is considered in the previous calculation and that stiffeners and their effect are not accounted for. Nevertheless, the F1 frequency of the resonators is tuned for enlarging the STL in the frequency band where it is found to be the lowest.

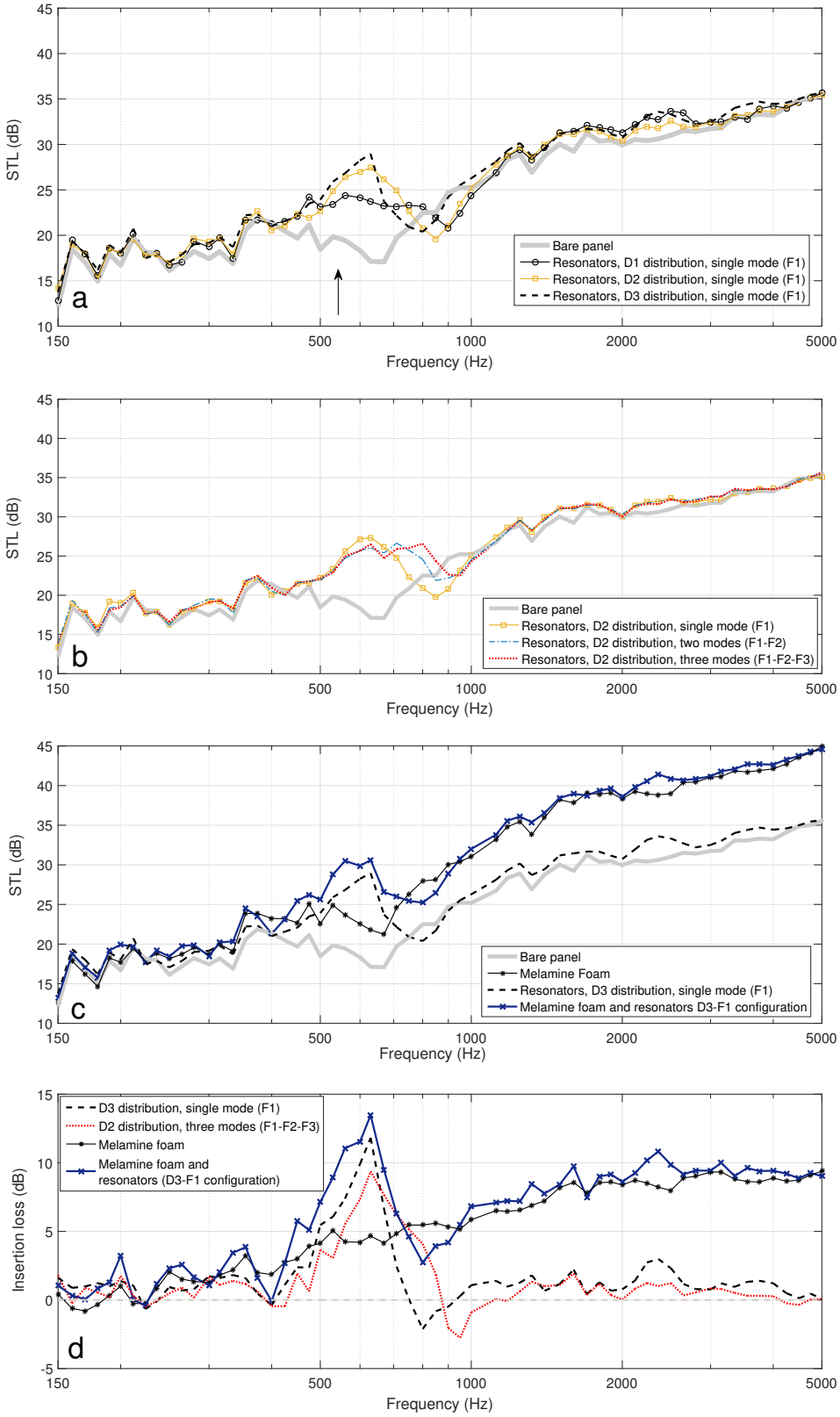

Fig. 3. (Color online) Summary of absolute and relative STL results obtained. (a) Effect of resonators distribution with single mode tuning (the ring-mode frequency is illustrated by a vertical arrow). (b) Effect of single to three-modes tuning with fixed distribution. (c) Separated and cumulative effect of melamine foam and resonators D3-F1 distribution. (d) Insertion loss (difference between considered solution and bare panel) for four key configurations.

The STL of the fuselage is measured before and after placing the resonators tuned on a single mode (F1, 670 Hz) with distributions D1, D2 and D3 (see Table 1). Corresponding results are provided in Figure 3(a). For the three distributions, the largest STL enhancements are not obtained in the 670 Hz twelfth octave band but in the preceding one, centered on a frequency of 630 Hz. Compared with the bare panel, the obtained STL gains for D1, D2 and D3 distributions are 6.6, 10.3 and 11.8 dB, respectively. The more concentrated D1 distribution produces a lower and smoother STL pic than when the resonators are more uniformly spread (*i.e.* D2 and D3 distributions). This result might indicate that local sound radiation is predominant around the ring mode's frequency bandwidth and that a spread spatial distribution of the resonators improves the sound insulation properties in the tuned frequency's bandwidth. This could also be a consequence of the spatial averaging done when measuring radiated sound intensity, that includes untreated bays in the case of the D1 distribution. The STL reduction observed around between 800 and 900 Hz in Fig. 3(a) is a known consequence of the tuned mass dampers anti-resonance. The dip nevertheless appears at different center frequencies depending on the considered D1, D2 or D3 distribution, with reduction of 5.1, 2.9 and 2.1 dB at twelfth octave bands frequencies of 900 Hz, 850 Hz and 800 Hz, respectively (with the bare panel result as a reference). Note that at the exception of this STL reduction, no other alteration of the sound insulation occurs in the 100-5000 Hz frequency range (see the result given in terms of insertion loss in Figure 3(d)).

In summary, results presented in Figure 3(a) indicate that the largest STL enlargements near the ring frequency (and the lowest alteration above) are reached with the D3

distribution. Nevertheless, the D2 distribution provides a good compromise in terms of overall STL improvement in the 500-800 Hz frequency range and is therefore chosen for studying the effect of different resonators frequencies. Combinations of F1, F2 and F3 resonators are used with D2 distribution and the obtained results are provided in Figure 3(b). Results show that the 2-modes and 3-modes configurations help limit the negative effect of the anti-resonance and enlarge the STL in the 800-950 Hz bandwidth. Compared with a single frequency configuration, the three modes configuration leads to an average STL improvement of 3.3 dB per 12^{th}-octave with a maximum of 5.7 dB at 800 Hz. This multi-resonant solution even reduces the add-on's weight from 5.7% to 4.9% (see Table 1). A multi-modal configuration of the resonators clearly increases the upper limit of the covered bandwidth from 750 Hz to 900 Hz. Interestingly, changing the frequency distribution within the fixed number of resonators does not modify the STL results in the rest of the frequency spectrum (see the result given in terms of insertion loss in Figure 3(d)).

In figure 3(c), the results for the D3-F1 configuration is recalled (see Figure 3(a)), and compared to the obtained results with the melamine foam alone and combined with the D3-F1 configuration. The addition of the foam treatment has for consequence an enlargement of the measured sound insulation starting at 250 Hz but nevertheless fails to fully compensate the STL loss resulting from the panel's ring mode as a result of its broadband behaviour (limited to a masking effect). When combined with the D3-F1 resonators configuration, the broadband effect of the melamine is almost additive to the narrow-band effect of the resonators. Compared with the foam alone case, the obtained STL result is enlarged at all

frequencies (at the exception of two STL reduction that can be found at 400 and 800 Hz frequencies). It is noteworthy that the additive effect is only limited at the peak enhancement brought by the resonators (see the result given in terms of insertion loss in Figure 3(d)). The maximum STL increase is found at the 630 Hz frequency band, with values of 11.8 and 13.5 dB for the foam alone and combined with the resonators, respectively.

5. Concluding remarks

The performance of a locally resonant solution for enlarging sound transmission loss of curved panels at ring frequency is demonstrated on an aircraft sidewall panel under a diffuse acoustic field excitation. The STL reduction occurring at and near the ring mode frequency is entirely suppressed with up to 10 dB gain with resonators tuned at a single frequency. The use of a multi-resonant configuration proves to be a solution for both enlarging the efficiency bandwidth and limiting the anti-resonance negative effect. It is finally demonstrated that the proposed concept can be combined with a broadband sound insulation treatment, the resonators' narrow-band and foam's broadband effects being nearly always additive in terms of STL benefits. Based on this first proof-of-concept, the on-going steps of this work are (1) a numerical model guiding an optimization of both the frequency tuning and number of resonators so as to be able to draw a 'cost function-like' map to propose reachable dB enhancements *vs* a target added mass, and (2) the design of a solution for plane panels so as to solve ring and coincidence frequency STL reductions. Finally, this compact and low-cost solution of 3D-printed small-scale cantilever beams could be also tested on arbitrarily shaped complex industrial-scale structures for solving other vibro-acoustic issues.

Acknowledgments

The help of Patrick Levesque at Université de Sherbrooke for the transmission loss experimental setup was greatly appreciated. The authors would also like to acknowledge Benoit Minard and Navdeep Sharma at Ecole Centrale de Lyon for their support in designing and manufacturing the resonators.

References and links

[1]B. Liu, L. Feng, and A. Nilsson, "Sound transmission through curved aircraft panels with stringer and ring frame attachments," J. Sound Vib. **300**, 949–973 (2007)

[2]T. Fu, Z. Chen, H. Yu, C. Li and X. Liu, "Optimization of sound transmission loss characteristics of orthogonally stiffened plate," J. Computational Acoustics **26**, 1850010 (2018).

[3]R. Boulandet, M. Michau, P. Micheau and A. Berry, "Aircraft panel with sensorless active sound power reduction through virtual mechanical impedances," J. Sound Vib. **361**, 2-19 (2016).

[4]M. Yuan, R. Ohayon, and J. Qiu, "Decentralized active control of turbulent boundary induced noise and vibration: a numerical investigation," J. Vib. Control, **22**(18), 3821–3839 (2016).

[5]O. Doutres, N. Atalla, and H. Osman, "Transfer matrix modeling and experimental validation of cellular porous material with resonant inclusions," J. Acoust. Soc. Am., **137**, 3502-3513 (2015).

[6]T. Yamamoto, "Acoustic metamaterial plate embedded with Helmholtz resonators for extraordinary sound transmission loss," J. Appl. Phys., **123**(21), 215110 (2018).

[7]Y. Song, L. Feng, J. Wen, D. Yu and X. Wen, "Reduction of the sound transmission of a periodic sandwich plate using the stop band concept," Compos. Struct., **128**, 428–436 (2015).

[8]Y. Xiao, J. Wen, and X. Wen, "Sound transmission loss of metamaterial-based thin plates with multiple subwavelength arrays of attached resonators, " J. Sound Vib., **331**(25), 5408-5423 (2012).

[9]Z. Liu, R. Rumpler, L. Feng, "Broadband locally resonant metamaterial sandwich plate for improved noise insulation in the coincidence region," Compos. Struct., **200**, 165–172 (2018).

[10]V. Romero-García, A. Krynkin, L.M. Garcia-Raffi, O. Umnova, and J.V. Sánchez-Pérez, "Multi-resonant scatterers in sonic crystals: Locally multi-resonant acoustic metamaterial" J. Sound Vib., **332**(1), 184–198 (2013).

[11]ISO15186-1:2000, *Acoustics – Measurement of sound insulation in buildings and of building elements using sound intensity – Part 1: Laboratory measurements* (International Standard Organization, Geneva, Switzerland, 2000).

[12]ASTM E2249 - 02 (2016), *Standard Test Method for Laboratory Measurement of Airborne Sound Transmission Loss of Building Partitions and Elements Using Sound Intensity* (ASTM International, West Conshohocken, PA, 2016).